ACS Photonics

pubs.acs.org/journal/apchd5

Article

Super-Poissonian Light Statistics from Individual Silicon Vacancy Centers Coupled to a Laser-Written Diamond Waveguide

Michael K. Koch, Michael Hoese, Vibhav Bharadwaj, Johannes Lang, John P. Hadden, Roberta Ramponi, Fedor Jelezko, Shane M. Eaton, and Alexander Kubanek*

Cite This: *ACS Photonics* 2022, 9, 3366−3373

Read Online

ACCESS | Metrics & More | Article Recommendations | Supporting Information

ABSTRACT: Modifying light fields at the single-photon level is a key challenge for upcoming quantum technologies and can be realized in a scalable manner through integrated quantum photonics. Laser-written diamond photonics offers 3D fabrication capabilities and large mode-field diameters matched to fiber optic technology, though limiting the cooperativity at the single-emitter level. To realize large coupling efficiencies, we combine excitation of single shallow-implanted silicon vacancy centers via high numerical aperture optics with detection assisted by laser-written type-II waveguides. We demonstrate single-emitter extinction measurements with a cooperativity of 0.0050 and a relative beta factor of 13%. The transmission of resonant photons reveals single-photon subtraction from a quasi-coherent field resulting in super-Poissonian light statistics. Our architecture enables light field engineering in an integrated design on the single quantum level although the intrinsic cooperativity is low. Laser-written structures can be fabricated in three dimensions and with a natural connectivity to optical fiber arrays.

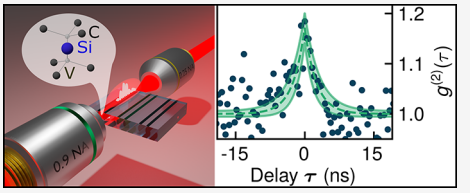

KEYWORDS: *laser writing, photonic engineering, integrated quantum optics, color center in diamond, quantum emitters*

Downloaded via 93.66.85.189 on February 3, 2023 at 08:46:09 (UTC).
See https://pubs.acs.org/sharingguidelines for options on how to legitimately share published articles.

INTRODUCTION

Color centers in diamond are an established platform for solid-state-based quantum communication and quantum sensing.[1] These color centers offer optically addressable electronic spin qubits,[2] access to nuclear spins,[3,4] which can serve as quantum memory,[5,6] and can be created in deterministic approaches.[7−9] Their potential for the realization of quantum networks is highlighted by the recent realization of a three-node quantum network with negatively charged nitrogen vacancy (NV^-) centers[10] and a quantum memory node with a negatively charged silicon vacancy (SiV^-) center.[11] Integration into photonic platforms with efficient coupling and access to a quantum optical non-linearity is a key challenge to facilitate scalability and robust operation for beyond-demonstrator implementation.[12] Diamond-based nanophotonics has reached the highest level of complexity,[13−15] including new design paths such as inverse engineering.[16] Working with photonics with larger mode-field diameters and therefore larger distance of the color center to the diamond surface would help to reduce the requirements on the fabrication process but inevitably lead to a reduced light−matter interaction strength prohibiting applications in the quantum regime. Another approach is hybrid quantum photonics, which offers the advantage of separate optimization of the photonics and the quantum emitter. However, the hybrid approach relies on elaborate manual functionalization.[17−19]

Ultrafast laser micromachining has emerged as a promising 3D fabrication technique for lab-on-a-chip quantum devices.[20] Laser-written photonic structures in diamond, based on type-II waveguides, offer a scalable pathway,[18] rapid fabrication, and enable compatibility with incorporation of color centers.[21] The laser-written waveguides can be adapted to a broad wavelength range and extended to more complex photonic structures such as beam splitters,[22] Bragg mirrors,[23] and 3D structures.[22,24] To functionalize the platform, NV^- centers have been created on demand by laser irradiation[25] or by shallow ion implantation into the front facet.[26] However, the intrinsic cooperativity of laser-written photonics is still low owing to the relatively large mode-field diameter, therefore prohibiting non-linear effects on the single-photon single-emitter level.

Here, we want to show that by exciting a SiV^- center via high numerical aperture (NA) optics we can observe non-linearities on the light field through a large mode volume waveguide. Therefore, we define a figure of merit adjusted to our architecture. The beta factor typically describes the fraction of overall emission coupled into the waveguide. Thus, we define a relative beta factor β_R which describes the ratio of the waveguide-coupled photon emission of the emitter to the waveguide-coupled excitation light. We overcome the limitation of intrinsic low cooperativities of laser-written photonics by exciting individual emitters with high NA optics

Received: May 20, 2022
Published: October 4, 2022

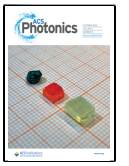

© 2022 The Authors. Published by American Chemical Society

whereas the detection is assisted by laser-written waveguides in diamond and a mode-matched low NA objective in transmission. This combination facilitates a high relative beta factor and, at the same time, efficient light field engineering on chip and in 3D waveguide arrays. We begin by functionalizing the waveguides with SiV^- centers, one of the group-IV color centers in diamond. They show a high coherent photon flux due to its high Debye–Waller factor,[27,28] an exceptional spectral stability thanks to its inversion symmetry[29,30] and coherent optical controllability of spin states.[31−33] Due to their strong interaction with light, single SiV^- centers can significantly modify weak light fields. We first perform extinction measurements to quantify the light–matter interaction on the single-emitter level. We then use the coupled system to subtract individual photons from a quasi-coherent light field resulting in a light field with super-Poissonian light statistics. Our results open the door for scalable, on-chip light field engineering on the single-photon level.

EXPERIMENTAL SECTION

Methods. We use laser-written type-II waveguides in an electronic grade diamond slab of dimensions $2 \times 2 \times 0.3$ mm^3. Each waveguide consists of two walls, indicated by the black lines in the sketch of the experimental setup as shown in Figure 1a,b. These walls are created by femtosecond laser writing[21,34,35] and are optimized for a transmission wavelength of 738 nm, corresponding to the zero phonon line (ZPL) wavelength of the SiV^- center. Similar to previous experiments with NV^- centers,[26] the defect centers are created by shallow ion implantation into the front facet of the waveguides (see Figure 1a).[36] In order to obtain spectrally stable emitters, we anneal the sample at 1000 °C after implantation. For more information on the implantation and annealing procedure, see the Supporting Information.

The presence of the waveguide walls induces strain on the SiV^- centers, which not only shifts the wavelength of the ZPL but also increases its ground-state and excited-state splitting.[37] The energy level scheme of the SiV^- center with its characteristic four-line structure (transition A–D) is shown in Figure 1c. The strain-induced shifts that we observe are also shown in this level scheme. We observe transverse strain leading to a ground- and excited-state splitting of 126 and 348 GHz, respectively, as well as longitudinal strain causing a shift of both orbital components.

The experimental setup, illustrated in Figure 1a,b, can be divided into two parts, the reflection and transmission path. A 0.25 NA objective aligned with one of the waveguides is used in the transmission path to collect the SiV^- emission coupled into the waveguide. We have confocal access via the reflection channel (0.9 NA), where the facet of the sample can be scanned using off-resonant 532 nm laser excitation or on-resonance with a tunable laser excitation source. The objectives are mounted on piezo scanners in the cryostat, but are not in thermal contact with the cold finger. Therefore, the setup is aligned after cooling and remains stable throughout the measurements. Both transmission and reflection paths can be used in a Hanbury Brown–Twiss (HBT) configuration to perform correlation measurements. All measurements are conducted at 5 K in a flow cryostat.

Device Characterization. First, we map the waveguide mode by scanning the high NA objective for excitation in the reflection path with a 738 nm laser and collect the coupled

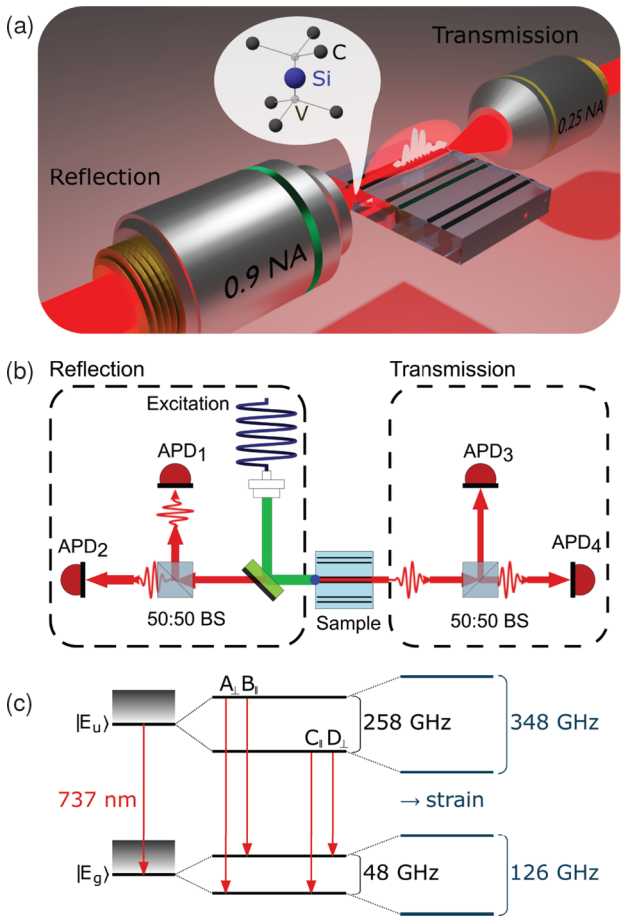

Figure 1. Experimental outline. (a) Schematic depiction of single photon coupling in the diamond waveguide. Here, the guidance of the excitation laser and the photon emission of a single shallow implanted SiV^- center is depicted. (b) Setup sketch, where a single SiV, indicated by the blue dot, is excited in the reflection path. Each detection path, in reflection and transmission, is equipped with two single photon detectors in HBT configuration. (c) Energy level structure of the utilized SiV^- defect center. Here, the ground- and excited-state splitting is shown for the zero strain case and the strain-induced splittings that we observe.

laser light via the transmission channel. The mode profile is depicted in Figure 2a, where the black vertical bars correspond to the walls of the waveguide. Next, we excite a single defect center resonantly using a 739.338 nm laser light, measured with a high precision wavemeter. The position of the defect center is indicated within the waveguide mode, together with a high-resolution confocal scan performed in reflection. The waveguides are polarization selective, due to the symmetry of the waveguide structure.[21] The polarization pattern of the waveguide (see Figure 2b), measured at the waveguide mode maximum, is aligned at $(170.5 \pm 2.4)°$. To test the polarization selectivity of the waveguide, we resonantly excite two different, spatially separated SiV^- defect centers (Line 1 and 2) near the transmission maximum of the waveguide and detect their respective phonon side bands (PSBs) in both detection channels. The detection in the reflection channel gives us the fluorescence signal independent of the waveguide transmission properties and allows us to compare it to the signal guided through the waveguide (transmission channel), which is polarization selected according to the waveguide properties. Accordingly, the polarization supported by the waveguide

https://doi.org/10.1021/acsphotonics.2c00774
ACS Photonics 2022, 9, 3366−3373

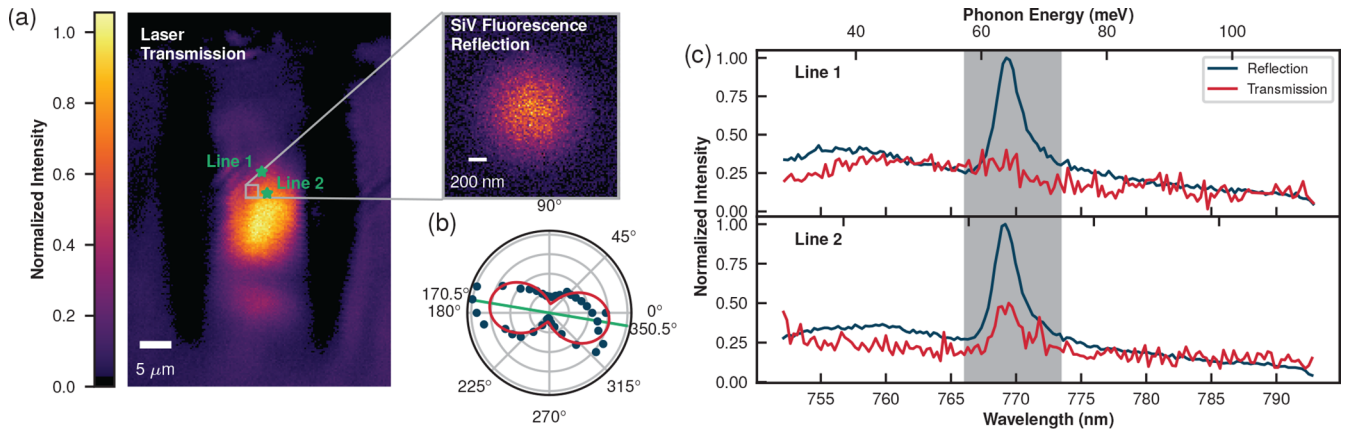

Figure 2. Device characterization. (a) Confocal scan (detected in transmission) of the waveguide, to map the waveguide mode. The laser wavelength is set to 738 nm and the polarization is set to the polarization of the waveguide. The inset shows a confocal scan of the SiV center in reflection at resonance (λ = 739.338 nm) and the markings reveal the position of the defect center within the waveguide. Also, the green stars mark the positions of Line 1 and 2. (b) Polarization dependence of the waveguide, measured in the same configuration as in part (a), but the laser is placed at the waveguide mode maximum. (c) Spectrum of the PSB for the PLE measurement for two different and spatially separated transitions, Line 1 at 738.404 nm and Line 2 at 738.327 nm, normalized in transmission to the reflection spectrum. The gray shaded area denotes the local mode at 64 meV.

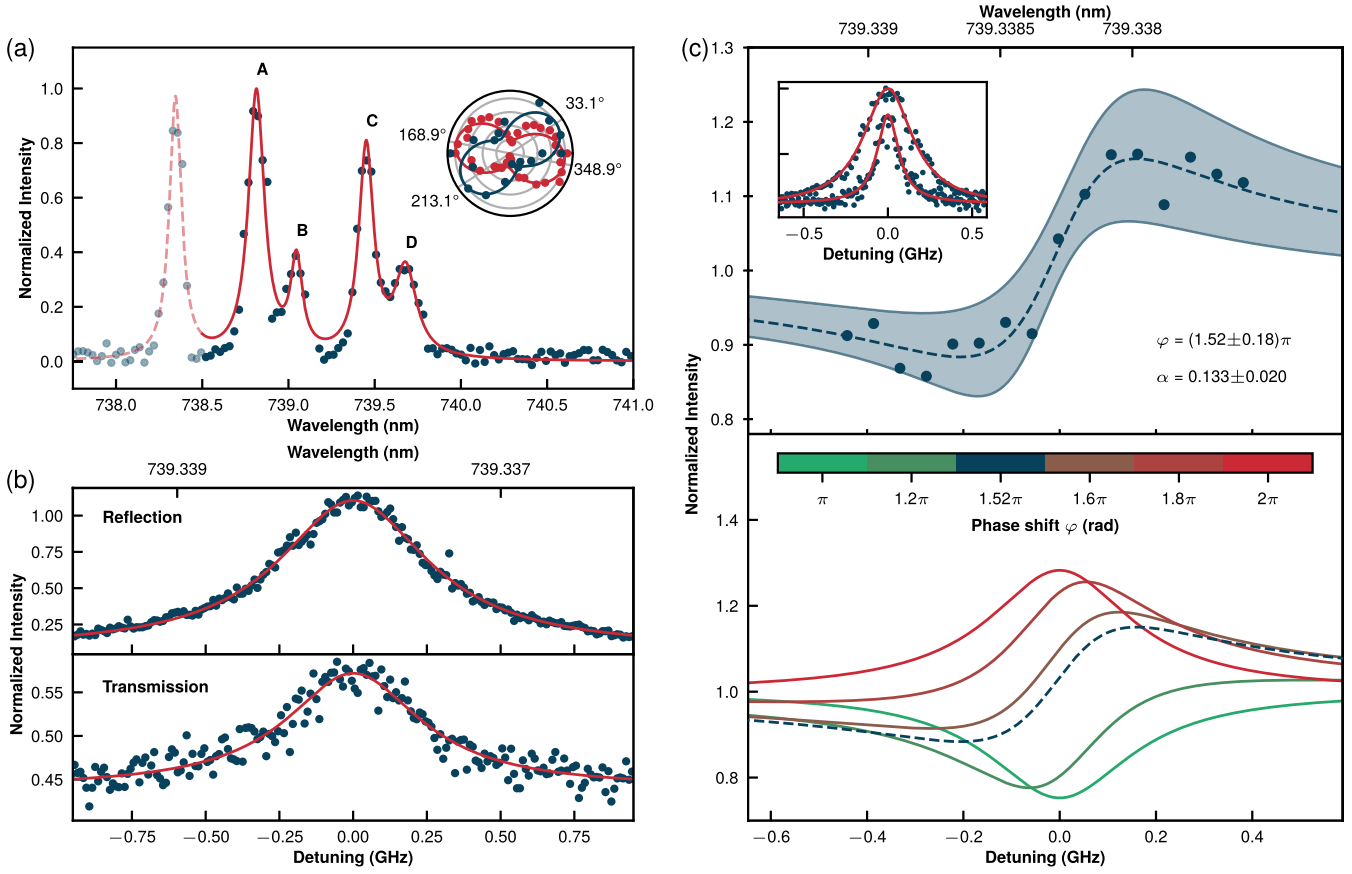

Figure 3. Resonant transmission (a) PL spectrum of the emitter (excited with 532 nm). The spectrum is background corrected and normalized to the maximum value of the corresponding fit function. The first peak in the spectrum, indicated by the dashed line, belongs to a second emitter within the confocal spot of the excitation laser. The inset polar plot shows the emission dipole of transition D (blue curve, off-resonantly excited) and the local mode (red curve, resonantly excited at 739.338 nm). (b) PLE scan of the emitter with a center wavelength of 739.338 nm detected in both the reflection and transmission channels. (c) Resonant transmission spectrum. The upper panel shows the measured transmission spectrum of the defect center waveguide system, where for each data point a 30 s count trace was recorded. Here, the dashed line is the resulting fit function fitted with eq 2 and the blue area represents the corresponding error margins with its 2σ confidence interval. In the inset, two PLE scans of the emitter are presented to show the effect of spectral diffusion, where one is quickly scanned over the resonance (narrow line) and the other scan took several minutes. In the lower panel, we show the expected behavior for the extinction measurement, when the relative phase of the local oscillator and the emitter is tuned from π to 2π, with our measurement (dashed line) as reference.

https://doi.org/10.1021/acsphotonics.2c00774
ACS Photonics 2022, 9, 3366−3373

transmission is more pronounced in the transmission signal. Two distinct features are the broad and the local mode with energy differences of 41 and 64 meV from the ZPL, respectively.[38] The measured PSBs of both Line 1 and 2, are shown in Figure 2c. In reflection, the PSB appears almost identical for both lines. In transmission, the local mode of Line 1 is much less visible compared to the 41 meV mode and the reflection signal. The local mode of Line 2, on the other hand, is transmitted much better, which means that Line 1 is polarized differently than Line 2. The PL spectrum of the SiV^- center is shown in Figure 3a. The labels A to D denote the transitions illustrated in Figure 1c. For resonant excitation, we use transition D. The polarization pattern for the emission dipole of transition D and the local mode is plotted in the inset of Figure 3a. Note that the polarization pattern of the local mode matches the waveguide polarization almost perfectly, whereas due to strain the polarization of transition D is tilted by 45°. For comparison and later analysis of the emitter coupling to the waveguide, we perform a PLE scan of transition D in reflection and transmission with a long scan time of 100 s, as shown in Figure 3b.

RESULTS AND DISCUSSION

Extinction Measurement. In the next step, we perform an extinction measurement on transition D where the guided excitation laser as well as the fluorescence is detected in transmission (see Figure 1a). We optimally align the polarization of the excitation laser to the polarization of transition D for an optimal excitation. The principle of this measurement is based on interference in the far field between the coherent excitation field (resonant laser) and coherent photons originating from resonant fluorescence (SiV^- center).[39] We use a 13 nm bandpass filter centered around 740 nm to select the coherent single photons from the ZPL transition, as well as the coherent laser photons. We sweep the laser frequency across transition D. The resulting interference effect is presented in the top panel of Figure 3c. Each data point in Figure 3c contains the averaged count rate of a 30 s count trace per frequency step. We neglect higher order modes that couple weakly to the waveguide and use the Ansatz of single mode interference between the driving field E_{DF} and the resonance fluorescence E_{RF} of the SiV^- center. In this picture, the resonance fluorescence field can be described as $E_{RF} = \beta_R S(\Delta) E_{DF} \exp(i\varphi)$ where β_R and φ are the relative weights between both fields and their relative phase, respectively.[40] The Lorentzian response of the fluorescence spectrum is given by

$$S(\Delta) = \frac{1}{1 - \frac{2i\Delta}{\gamma}} \tag{1}$$

where Δ describes the frequency detuning from the resonance and γ is the FWHM of the fluorescence line shape. Therefore, the detected intensity I_{det} is proportional to

$$I_{det}(\Delta) \propto |1 + \beta_R S(\Delta) \exp(i\varphi)|^2 \tag{2}$$

which we use to fit the data as illustrated in Figure 3c. Due to the long measurement time, the resulting dispersive line shape contains the inhomogeneous linewidth of the emission line as seen in the inset of Figure 3c. The measurement time for the displayed PLE scans is 3.5 and 100 s for the narrow and the broad PLE line in the inset, respectively, according to a linewidth of (154 ± 7) and (354 ± 9) MHz, respectively. With the fit model from eq 2, we obtain a FWHM of (360 ± 60) MHz and a phase shift of $(1.52 \pm 0.18)\pi$, which is the maximally dispersive case.

We use excitation powers of 400 fW, well below the saturation powers reported for SiV centers in bulk diamond.[41,42] Therefore, the condition for low power $\Omega_c/\Gamma = 0.00249 \ll 1$ is satisfied where Ω_c is the Rabi frequency and Γ is the fluorescence decay rate. To simulate the expected behavior of our system for different phase shifts φ, we extrapolate the relative phase in eq 2 from π to 2π, see lower panel of Figure 3c. By considering the relative phase of π, which represents the absorptive case, we can extract the value of the transmission intensity at resonance $T = 0.75 \pm 0.04$ with a relative beta factor of $\beta_R = 0.133 \pm 0.020$. By taking the laser coupling efficiency to the waveguide (0.114) and the positional (0.607) as well as the polarizational (0.542) mismatch into account, we derive the beta factor for the emitter-waveguide coupling to be $\beta = 0.0050 \pm 0.0012$. The beta factor, β, given by

$$\beta = \frac{C}{1 + C} \tag{3}$$

effectively describes the coupling efficiency of the SiV^- center's photon emission into the waveguide where C is the cooperativity. This results in a cooperativity of $C = 0.0050 \pm 0.0013$, which describes a lower bound for the quantum efficiency (QE) of the investigated emitter[40] because the line broadening and the ZPL branching ratio[40,43] have an effect on the cooperativity, but not on the QE. Taking into account all factors that affect the coupling efficiency but not the QE, namely the position (0.61) and polarization mismatch (0.54), the branching ratio into the ZPL (0.8) and the line broadening (0.43), we obtain a lower bound of 4.4% for the QE. The lower limit for the QE determined in this way is in agreement with values from previous reports for SiVs in bulk diamond.[14,44,45] As depicted in Figure 3c, we observe a broadened inhomogeneous linewidth due to spectral diffusion (154 MHz/360 MHz ≈ 0.43). The relative intensities found for the PLE measurement in transmission and reflection, compare to Figure 3b, lead to a relative coupling efficiency of $\eta_{rel} = 0.115 \pm 0.007$ and are in agreement with the results of a previous study.[26] By accounting for the differences (0.8/0.6) in detection efficiency for each path and considering the absolute detection efficiency of the post-objective confocal collection (0.025), this also serves as a sanity check for the beta factor. We obtain a beta factor and cooperativity of $\beta = 0.0038 \pm 0.0004$ and $C = 0.0039 \pm 0.0004$, respectively, which are consistent with the previously derived values. Although this value was determined more precisely, it only serves to verify the previously stated values for the beta factor and cooperativity because it only takes the coupling of the PSB to the waveguide into account and not the coherent photons of the ZPL. In summary, despite the intrinsically low cooperativity of the laser-written waveguide due to the relatively large mode-field diameter, our architecture enables the observation of single-atom single-photon non-linearities based on a reasonably high relative beta factor.

Super-Poissonian Light Statistics by Single Photon Absorption. Now we turn to the quantum non-linear character of the SiV^--waveguide system. We measure the autocorrelation of the transmitted signal in the HBT configuration. First, we measure the autocorrelation in reflection by exciting the defect center at resonance with a

https://doi.org/10.1021/acsphotonics.2c00774
ACS Photonics 2022, 9, 3366−3373

power of 450 nW and detecting only the PSB (see Figure 4a). Because $g^{(2)}(0)$ is well below the threshold of 0.5 for a single

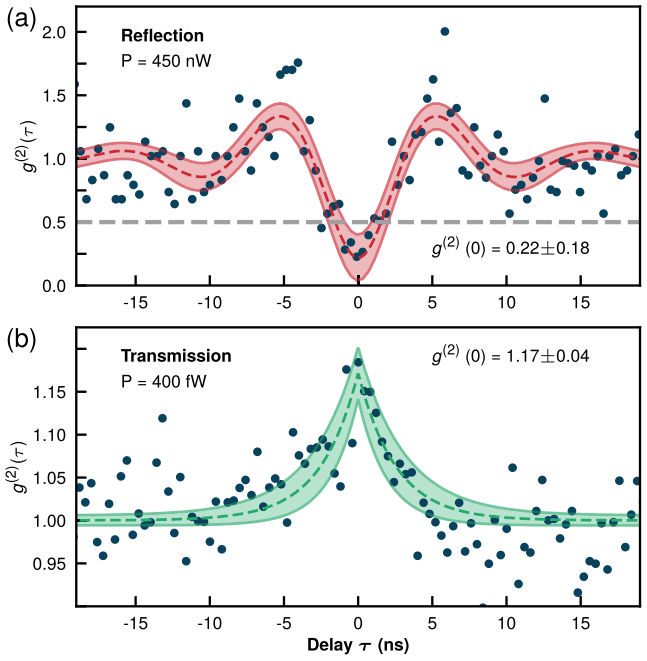

Figure 4. Second-order correlation measurements in reflection and transmission. (a) Results of a second-order correlation measurement in reflection at resonance (739.338 nm) with a SiV^- center ZPL transition, where only PSB photons are detected. Here, a fitted value of $g^{(2)}(0) = 0.22 \pm 0.18$ which is <0.5 corresponds to single photon emission by the defect center. (b) Correlation measurement at resonance with the same transition, detected in transmission (740/13 nm BP). Here, the quasi-coherent laser light is correlated with the emitters' fluorescence, which is guided through the waveguide (compare to Figure 1b). At zero time delay, bunching is clearly visible. The determined error margins, including the 2σ confidence interval, are indicated by the highlighted red and green areas, respectively.

photon emitter, we conclude that only a single defect center is excited. The transmission signal, obtained under identical conditions as the extinction measurement but excited with a quasi-coherent field (excitation power of 400 fW) as shown in Figure 3c, should now be modified by the single photon transition of the SiV^- center. In order to investigate the effect on the photon statistics, we work with sufficiently low laser powers, so that the driving field is a quasi-coherent state with non-negligible single- and two-photon contribution. A measured power of $P_0 = (470 \pm 24)$ nW yields (240 ± 12) fW after attenuation (ND = 6.3). Considering the photon statistics of a quasi-coherent light field, the mean photon number $\langle n\rangle_\tau$ within the given excited-state lifetime of the emitter $\tau_{ex} = (2.5 \pm 0.6)$ ns is determined by $\langle n\rangle_\tau = P_0\eta_{tot}\tau_{ex}/h\nu$ where η_{tot} is the total attenuation, h is the Planck constant, and ν is the laser frequency. This yields a mean photon number of $\langle n\rangle_\tau = 0.0022 \pm 0.0007$ for the quasi-coherent field and an eigenvalue of $\alpha = \sqrt{\langle n\rangle_\tau} = 0.047 \pm 0.007$. Hence, the quasi-coherent state, normalized to the lifetime of the emitter, is described by

$$|\alpha\rangle = e^{-|\alpha|^2/2}\sum_{n=0}^{\infty}\frac{\alpha^n}{\sqrt{n!}}|n\rangle$$
$$= 0.9989|0\rangle + 0.0472|1\rangle + 0.0016|2\rangle + \ldots$$

In the case of large photon−atom interaction, a low photon flux of the excitation field can saturate the defect center's transition and a single SiV^- center can modify the output field. Consequently, single photons are removed from the quasi-coherent state resulting in a super-Poissonian light statistic of the transmitted light. In this case, a bunching behavior at zero time delay is expected in the HBT correlation measurement, as confirmed by the autocorrelation measurement presented in Figure 4b. We use

$$g^{(2)}(\tau) = 1 - ae^{-3\Gamma|\tau|/4}\left(\cos\Omega_\Gamma|\tau| + \frac{3\Gamma}{4\Omega_\Gamma}\sin\Omega_\Gamma|\tau|\right) \quad (4)$$

to fit the antibunching curve in Figure 4a because we excite the transition with a strong driving field,[46] where Γ is the emitters' fluorescence decay rate, $\Omega_\Gamma = (\Omega_c^2 - (\Gamma/4)^2)^{0.5}$ is the damped Rabi frequency, and Ω_c is the Rabi frequency. To evaluate the bunching behavior in the transmission measurement as shown in Figure 4b, we use the fit function

$$g^{(2)}(\tau) = 1 + ae^{-\Gamma|\tau|} \quad (5)$$

because we operate at a low driving power well below saturation. At zero time delay, we get $g^{(2)}(0) = 1.17 \pm 0.04$. The bunching behavior is confirmed by two other measurements, as shown in the Supporting Information. As control, we measure the correlation function for the laser far detuned from resonance of the emitter which results in a flat line, with $g^{(2)}(\tau) = 1$ as expected for a quasi-coherent state (see the Supporting Information). With that, we can confirm that the observed super-Poissonian light statistic of the investigated defect center is the result of single photon interference in the far field (detector location).[40,43,47]

CONCLUSIONS

In summary, by combining high NA excitation with waveguide-assisted detection, we achieve a high relative beta factor for laser-written diamond photonics despite their otherwise low overall beta factor due to the large mode-field diameter. The observed coupling to our laser-written waveguide system opens the possibility to work with group-IV defects in diamond at the single-photon level. We present evidence for a single photon non-linearity in a laser-written SiV^--waveguide system, where the non-linearity arises from the interaction between the quasi-coherent excitation field and the resonant fluorescence of the defect center. We perform an extinction measurement on the SiV^--waveguide system in order to extract the cooperativity of $C = 0.0050$. Furthermore, we probe the polarization selectivity of the system. Ultimately, we demonstrate super-Poissonian light statistics originating from single photon subtraction of a quasi-coherent light field. This opens a new path to the longstanding goal to engineer light at the single-photon level. The reported device is an on-chip proof-of-principle architecture combining ultrafast laser-written waveguides with single SiV emitter for single photon manipulation. The demonstrated device paves a path toward 3D integrated photonics in diamond enabled by ultrafast laser writing where complex quantum networks can be realized within the bulk of diamond. In the future, controlling the phase between

https://doi.org/10.1021/acsphotonics.2c00774
ACS Photonics 2022, 9, 3366−3373

excitation and emission paths will further enable switching between single photon subtraction and addition leading to the engineering of arbitrary, nonclassical light fields.[48] The nonclassical light field engineering could build on the ability to laser-write advanced photonic components such as Y-beam splitter and Bragg gratings[22,23] and benefit from the three-dimensional writing capabilities. Functionalization of multiple waveguides by wide-field implantation of the front facet enables scalable quantum technology and good optical access via standard optical fibers for detection while maintaining the high NA excitation configuration. Extending Y-beam splitters to X-beam splitter facilitates, together with the high degree of indistinguishability of single photons emitted from SiV^- centers, on-chip Hong-Ou-Mandel interference[30] and the construction of path-entangled light fields for applications in quantum metrology, such as super-resolution phase estimation beyond the standard quantum limit.[49]

■ ASSOCIATED CONTENT

Supporting Information

The Supporting Information is available free of charge at https://pubs.acs.org/doi/10.1021/acsphotonics.2c00774.

> Waveguide fabrication; SiV^- center creation; control measurement for super-Poissonian light statistics; and discussion on the fit function of the resonant correlation measurement in transmission (PDF)

■ AUTHOR INFORMATION

Corresponding Author

Alexander Kubanek − *Institute for Quantum Optics and Center for Integrated Quantum Science and Technology (IQst), Ulm University, Ulm D-89081, Germany;* orcid.org/0000-0002-2417-1985; Email: alexander.kubanek@uni-ulm.de

Authors

Michael K. Koch − *Institute for Quantum Optics and Center for Integrated Quantum Science and Technology (IQst), Ulm University, Ulm D-89081, Germany;* orcid.org/0000-0002-7998-9530

Michael Hoese − *Institute for Quantum Optics, Ulm University, Ulm D-89081, Germany;* orcid.org/0000-0001-7820-487X

Vibhav Bharadwaj − *Institute for Photonics and Nanotechnologies (IFN)—CNR, Milano 20133, Italy; Institute for Quantum Optics, Ulm University, Ulm D-89081, Germany*

Johannes Lang − *Institute for Quantum Optics, Ulm University, Ulm D-89081, Germany; Diatope GmbH, Ummendorf D-88444, Germany*

John P. Hadden − *School of Physics and Astronomy, Cardiff University, Cardiff CF24 3AA, U.K.;* orcid.org/0000-0001-5407-6754

Roberta Ramponi − *Institute for Photonics and Nanotechnologies (IFN)—CNR, Milano 20133, Italy*

Fedor Jelezko − *Institute for Quantum Optics and Center for Integrated Quantum Science and Technology (IQst), Ulm University, Ulm D-89081, Germany*

Shane M. Eaton − *Institute for Photonics and Nanotechnologies (IFN)—CNR, Milano 20133, Italy*

Complete contact information is available at: https://pubs.acs.org/10.1021/acsphotonics.2c00774

Author Contributions

M.K.K. and M.H. contributed equally to this work. M.K.K., M.H., V.B., S.M.E., and A.K. conceived the project. M.K.K. and M.H. performed and analyzed all PL, PLE, and correlation measurements. V.B., J.P.H., R.R., and S.M.E. produced the laser-written waveguides in diamond, which were implanted and annealed by J.L. and F.J. to create SiV^- centers. All authors discussed the results. M.K.K., M.H., and A.K. wrote the manuscript, which was discussed and edited by all authors.

Funding

IFN-CNR and UUlm were supported by the H2020 Marie Curie ITN project LasIonDef (GA no. 956387). IFN-CNR was supported by the project QuantDia (FISR2019-05178) funded by Ministero dell'Istruzione, dell'Università e della Ricerca. A.K. was supported by the European Regional Development Fund (EFRE) program Baden-Württemberg. M.K.K. and A.K. were supported by the IQst. M.H. was supported by the Studienstiftung des deutschen Volkes. V.B. was supported by the Alexander von Humboldt Foundation.

Notes

The authors declare no competing financial interest.

■ ACKNOWLEDGMENTS

The authors thank Felix Breuning for experimental support in the beginning of the project.

■ REFERENCES

(1) Atatüre, M.; Englund, D.; Vamivakas, N.; Lee, S.-Y.; Wrachtrup, J. Material platforms for spin-based photonic quantum technologies. *Nat. Rev. Mater.* **2018**, *3*, 38−51.

(2) Awschalom, D. D.; Hanson, R.; Wrachtrup, J.; Zhou, B. B. Quantum technologies with optically interfaced solid-state spins. *Nat. Photonics* **2018**, *12*, 516−527.

(3) Neumann, P.; Beck, J.; Steiner, M.; Rempp, F.; Fedder, H.; Hemmer, P. R.; Wrachtrup, J.; Jelezko, F. Single-Shot Readout of a Single Nuclear Spin. *Science* **2010**, *329*, 542−544.

(4) Metsch, M. H.; Senkalla, K.; Tratzmiller, B.; Scheuer, J.; Kern, M.; Achard, J.; Tallaire, A.; Plenio, M. B.; Siyushev, P.; Jelezko, F. Initialization and Readout of Nuclear Spins via a Negatively Charged Silicon-Vacancy Center in Diamond. *Phys. Rev. Lett.* **2019**, *122*, 190503.

(5) Maurer, P. C.; Kucsko, G.; Latta, C.; Jiang, L.; Yao, N. Y.; Bennett, S. D.; Pastawski, F.; Hunger, D.; Chisholm, N.; Markham, M.; Twitchen, D. J.; Cirac, J. I.; Lukin, M. D. Room-Temperature Quantum Bit Memory Exceeding One Second. *Science* **2012**, *336*, 1283−1286.

(6) Bradley, C. E.; Randall, J.; Abobeih, M. H.; Berrevoets, R. C.; Degen, M. J.; Bakker, M. A.; Markham, M.; Twitchen, D. J.; Taminiau, T. H. A Ten-Qubit Solid-State Spin Register with Quantum Memory up to One Minute. *Phys. Rev. X* **2019**, *9*, 031045.

(7) Evans, R. E.; Sipahigil, A.; Sukachev, D. D.; Zibrov, A. S.; Lukin, M. D. Narrow-Linewidth Homogeneous Optical Emitters in Diamond Nanostructures via Silicon Ion Implantation. *Appl. Phys. Rev.* **2016**, *5*, 044010.

(8) Chen, Y.-C.; Salter, P. S.; Knauer, S.; Weng, L.; Frangeskou, A. C.; Stephen, C. J.; Ishmael, S. N.; Dolan, P. R.; Johnson, S.; Green, B. L.; et al. Laser writing of coherent colour centres in diamond. *Nat. Photonics* **2017**, *11*, 77−80.

(9) Schröder, T.; Trusheim, M. E.; Walsh, M.; Li, L.; Zheng, J.; Schukraft, M.; Sipahigil, A.; Evans, R. E.; Sukachev, D. D.; Nguyen, C. T.; Pacheco, J. L.; Camacho, R. M.; Bielejec, E. S.; Lukin, M. D.; Englund, D. Scalable focused ion beam creation of nearly lifetime-limited single quantum emitters in diamond nanostructures. *Nat. Commun.* **2017**, *8*, 15376.

(10) Pompili, M.; Hermans, S. L. N.; Baier, S.; Beukers, H. K. C.; Humphreys, P. C.; Schouten, R. N.; Vermeulen, R. F. L.; Tiggelman,

M. J.; dos Santos Martins, L.; Dirkse, B.; Wehner, S.; Hanson, R. Realization of a multinode quantum network of remote solid-state qubits. *Science* **2021**, *372*, 259−264.
(11) Bhaskar, M. K.; Riedinger, R.; Machielse, B.; Levonian, D. S.; Nguyen, C. T.; Knall, E. N.; Park, H.; Englund, D.; Lončar, M.; Sukachev, D. D.; et al. Experimental demonstration of memory-enhanced quantum communication. *Nature* **2020**, *580*, 60−64.
(12) Ruf, M.; Wan, N. H.; Choi, H.; Englund, D.; Hanson, R. Quantum networks based on color centers in diamond. *J. Appl. Phys.* **2021**, *130*, 070901.
(13) Hausmann, B. J. M.; Shields, B.; Quan, Q.; Maletinsky, P.; McCutcheon, M.; Choy, J. T.; Babinec, T. M.; Kubanek, A.; Yacoby, A.; Lukin, M. D.; Lončar, M. Integrated Diamond Networks for Quantum Nanophotonics. *Nano Lett.* **2012**, *12*, 1578−1582.
(14) Riedrich-Möller, J.; Arend, C.; Pauly, C.; Mücklich, F.; Fischer, M.; Gsell, S.; Schreck, M.; Becher, C. Deterministic Coupling of a Single Silicon-Vacancy Color Center to a Photonic Crystal Cavity in Diamond. *Nano Lett.* **2014**, *14*, 5281−5287.
(15) Zhang, J. L.; Sun, S.; Burek, M. J.; Dory, C.; Tzeng, Y.-K.; Fischer, K. A.; Kelaita, Y.; Lagoudakis, K. G.; Radulaski, M.; Shen, Z.-X.; Melosh, N. A.; Chu, S.; Lončar, M.; Vučković, J. Strongly Cavity-Enhanced Spontaneous Emission from Silicon-Vacancy Centers in Diamond. *Nano Lett.* **2018**, *18*, 1360−1365.
(16) Dory, C.; Vercruysse, D.; Yang, K. Y.; Sapra, N. V.; Rugar, A. E.; Sun, S.; Lukin, D. M.; Piggott, A. Y.; Zhang, J. L.; Radulaski, M.; Lagoudakis, K. G.; Su, L.; Vučković, J. Inverse-designed diamond photonics. *Nat. Commun.* **2019**, *10*, 3309.
(17) Schrinner, P. P. J.; Olthaus, J.; Reiter, D. E.; Schuck, C. Integration of Diamond-Based Quantum Emitters with Nanophotonic Circuits. *Nano Lett.* **2020**, *20*, 8170−8177.
(18) Wan, N. H.; Lu, T.-J.; Chen, K. C.; Walsh, M. P.; Trusheim, M. E.; De Santis, L.; Bersin, E. A.; Harris, I. B.; Mouradian, S. L.; Christen, I. R.; et al. Large-scale integration of artificial atoms in hybrid photonic circuits. *Nature* **2020**, *583*, 226−231.
(19) Fehler, K. G.; Antoniuk, L.; Lettner, N.; Ovvyan, A. P.; Waltrich, R.; Gruhler, N.; Davydov, V. A.; Agafonov, V. N.; Pernice, W. H. P.; Kubanek, A. Hybrid Quantum Photonics Based on Artificial Atoms Placed Inside One Hole of a Photonic Crystal Cavity. *ACS Photonics* **2021**, *8*, 2635−2641.
(20) Corrielli, G.; Crespi, A.; Osellame, R. Femtosecond laser micromachining for integrated quantum photonics. *Nanophotonics* **2021**, *10*, 3789−3812.
(21) Sotillo, B.; et al. Diamond photonics platform enabled by femtosecond laser writing. *Sci. Rep.* **2016**, *6*, 35566.
(22) Courvoisier, A.; Booth, M. J.; Salter, P. S. Inscription of 3D waveguides in diamond using an ultrafast laser. *Appl. Phys. Lett.* **2016**, *109*, 031109.
(23) Bharadwaj, V.; Courvoisier, A.; Fernandez, T. T.; Ramponi, R.; Galzerano, G.; Nunn, J.; Booth, M. J.; Osellame, R.; Eaton, S. M.; Salter, P. S. Femtosecond laser inscription of Bragg grating waveguides in bulk diamond. *Opt. Lett.* **2017**, *42*, 3451.
(24) Kononenko, T.; Konov, V.; Pimenov, S.; Rossukanyi, N.; Rukovishnikov, A.; Romano, V. Three-dimensional laser writing in diamond bulk. *Diamond Relat. Mater.* **2011**, *20*, 264−268.
(25) Hadden, J. P.; Bharadwaj, V.; Sotillo, B.; Rampini, S.; Osellame, R.; Witmer, J. D.; Jayakumar, H.; Fernandez, T. T.; Chiappini, A.; Armellini, C.; Ferrari, M.; Ramponi, R.; Barclay, P. E.; Eaton, S. M. Integrated waveguides and deterministically positioned nitrogen vacancy centers in diamond created by femtosecond laser writing. *Opt. Lett.* **2018**, *43*, 3586.
(26) Hoese, M.; Koch, M. K.; Bharadwaj, V.; Lang, J.; Hadden, J. P.; Yoshizaki, R.; Giakoumaki, A. N.; Ramponi, R.; Jelezko, F.; Eaton, S. M.; Kubanek, A. Integrated Magnetometry Platform with Stackable Waveguide-Assisted Detection Channels for Sensing Arrays. *Phys. Rev. Appl.* **2021**, *15*, 054059.
(27) Neu, E.; Steinmetz, D.; Riedrich-Möller, J.; Gsell, S.; Fischer, M.; Schreck, M.; Becher, C. Single photon emission from silicon-vacancy colour centres in chemical vapour deposition nano-diamonds on iridium. *New J. Phys.* **2011**, *13*, 025012.
(28) Dietrich, A.; Jahnke, K. D.; Binder, J. M.; Teraji, T.; Isoya, J.; Rogers, L. J.; Jelezko, F. Isotopically varying spectral features of silicon-vacancy in diamond. *New J. Phys.* **2014**, *16*, 113019.
(29) Rogers, L. J.; Jahnke, K. D.; Teraji, T.; Marseglia, L.; Müller, C.; Naydenov, B.; Schauffert, H.; Kranz, C.; Isoya, J.; McGuinness, L. P.; et al. Multiple intrinsically identical single-photon emitters in the solid state. *Nat. Commun.* **2014**, *5*, 4739.
(30) Sipahigil, A.; Jahnke, K. D.; Rogers, L. J.; Teraji, T.; Isoya, J.; Zibrov, A. S.; Jelezko, F.; Lukin, M. D. Indistinguishable Photons from Separated Silicon-Vacancy Centers in Diamond. *Phys. Rev. Lett.* **2014**, *113*, 113602.
(31) Rogers, L. J.; Jahnke, K. D.; Metsch, M. H.; Sipahigil, A.; Binder, J. M.; Teraji, T.; Sumiya, H.; Isoya, J.; Lukin, M. D.; Hemmer, P.; Jelezko, F. All-Optical Initialization, Readout, and Coherent Preparation of Single Silicon-Vacancy Spins in Diamond. *Phys. Rev. Lett.* **2014**, *113*, 263602.
(32) Pingault, B.; Jarausch, D.-D.; Hepp, C.; Klintberg, L.; Becker, J. N.; Markham, M.; Becher, C.; Atatüre, M. Coherent control of the silicon-vacancy spin in diamond. *Nat. Commun.* **2017**, *8*, 1−7.
(33) Becker, J. N.; Pingault, B.; Groß, D.; Gündoğan, M.; Kukharchyk, N.; Markham, M.; Edmonds, A.; Atatüre, M.; Bushev, P.; Becher, C. All-Optical Control of the Silicon-Vacancy Spin in Diamond at Millikelvin Temperatures. *Phys. Rev. Lett.* **2018**, *120*, 053603.
(34) Eaton, S. M.; Hadden, J. P.; Bharadwaj, V.; Forneris, J.; Picollo, F.; Bosia, F.; Sotillo, B.; Giakoumaki, A. N.; Jedrkiewicz, O.; Chiappini, A.; Ferrari, M.; Osellame, R.; Barclay, P. E.; Olivero, P.; Ramponi, R. Quantum Micro−Nano Devices Fabricated in Diamond by Femtosecond Laser and Ion Irradiation. *Adv. Quantum Technol.* **2019**, *2*, 1900006.
(35) Bharadwaj, V.; Jedrkiewicz, O.; Hadden, J. P.; Sotillo, B.; Vázquez, M. R.; Dentella, P.; Fernandez, T. T.; Chiappini, A.; Giakoumaki, A. N.; Le Phu, T.; Bollani, M.; Ferrari, M.; Ramponi, R.; Barclay, P. E.; Eaton, S. M. Femtosecond laser written photonic and microfluidic circuits in diamond. *J. Phys.: Photonics* **2019**, *1*, 022001.
(36) Lang, J.; Häußler, S.; Fuhrmann, J.; Waltrich, R.; Laddha, S.; Scharpf, J.; Kubanek, A.; Naydenov, B.; Jelezko, F. Long optical coherence times of shallow-implanted, negatively charged silicon vacancy centers in diamond. *Appl. Phys. Lett.* **2020**, *116*, 064001.
(37) Meesala, S.; et al. Strain engineering of the silicon-vacancy center in diamond. *Phys. Rev. B* **2018**, *97*, 205444.
(38) Rogers, L. J.; Jahnke, K. D.; Doherty, M. W.; Dietrich, A.; McGuinness, L. P.; Müller, C.; Teraji, T.; Sumiya, H.; Isoya, J.; Manson, N. B.; Jelezko, F. Electronic structure of the negatively charged silicon-vacancy center in diamond. *Phys. Rev. B: Condens. Matter Mater. Phys.* **2014**, *89*, 235101.
(39) Wrigge, G.; Gerhardt, I.; Hwang, J.; Zumofen, G.; Sandoghdar, V. Efficient coupling of photons to a single molecule and the observation of its resonance fluorescence. *Nat. Phys.* **2008**, *4*, 60−66.
(40) Bhaskar, M.; Sukachev, D.; Sipahigil, A.; Evans, R.; Burek, M.; Nguyen, C.; Rogers, L.; Siyushev, P.; Metsch, M.; Park, H.; Jelezko, F.; Lončar, M.; Lukin, M. Quantum Nonlinear Optics with a Germanium-Vacancy Color Center in a Nanoscale Diamond Waveguide. *Phys. Rev. Lett.* **2017**, *118*, 223603.
(41) Häußler, S.; Thiering, G.; Dietrich, A.; Waasem, N.; Teraji, T.; Isoya, J.; Iwasaki, T.; Hatano, M.; Jelezko, F.; Gali, A.; Kubanek, A. Photoluminescence excitation spectroscopy of SiV-and GeV-color center in diamond. *New J. Phys.* **2017**, *19*, 063036.
(42) Li, K.; Zhou, Y.; Rasmita, A.; Aharonovich, I.; Gao, W. Nonblinking Emitters with Nearly Lifetime-Limited Linewidths in CVD Nanodiamonds. *Phys. Rev. Appl.* **2016**, *6*, 024010.
(43) Chang, D. E.; Sørensen, A. S.; Demler, E. A.; Lukin, M. D. A single-photon transistor using nanoscale surface plasmons. *Nat. Phys.* **2007**, *3*, 807−812.
(44) Sipahigil, A.; et al. An integrated diamond nanophotonics platform for quantum-optical networks. *Science* **2016**, *354*, 847−850.
(45) Becker, J. N.; Becher, C. Coherence Properties and Quantum Control of Silicon Vacancy Color Centers in Diamond. *Phys. Status Solidi* **2017**, *214*, 1700586.

https://doi.org/10.1021/acsphotonics.2c00774
ACS Photonics 2022, 9, 3366−3373

(46) Steck, D. A.Quantum and Atom Optics, 2007, Revision 0.13.10, 22 September 2021. available online at http://steck.us/teaching (accessed on Oct 29, 2021).
(47) Javadi, A.; Söllner, I.; Arcari, M.; Hansen, S. L.; Midolo, L.; Mahmoodian, S.; Kiršanskė, G.; Pregnolato, T.; Lee, E. H.; Song, J. D.; Stobbe, S.; Lodahl, P. Single-photon non-linear optics with a quantum dot in a waveguide. *Nat. Commun.* **2015**, *6*, 8655.
(48) Du, J.; Li, W.; Bajcsy, M. Deterministic single-photon subtraction based on a coupled single quantum dot-cavity system. *Opt. Express* **2020**, *28*, 6835−6845.
(49) Polino, E.; Valeri, M.; Spagnolo, N.; Sciarrino, F. Photonic quantum metrology. *AVS Quantum Sci.* **2020**, *2*, 024703.

Recommended by ACS

Silicon Nitride Waveguides with Intrinsic Single-Photon Emitters for Integrated Quantum Photonics
Alexander Senichev, Vladimir M. Shalaev, *et al.*
SEPTEMBER 13, 2022
ACS PHOTONICS
READ

Low-Divergence hBN Single-Photon Source with a 3D-Printed Low-Fluorescence Elliptical Polymer Microlens
Johann A. Preuß, Rudolf Bratschitsch, *et al.*
NOVEMBER 29, 2022
NANO LETTERS
READ

Multiobjective Inverse Design of Solid-State Quantum Emitter Single-Photon Sources
Emerson G. Melo, Marcelo Davanco, *et al.*
SEPTEMBER 19, 2022
ACS PHOTONICS
READ

High-Performance Single-Photon Sources at Telecom Wavelength Based on Broadband Hybrid Circular Bragg Gratings
Andrea Barbiero, Andrew J. Shields, *et al.*
AUGUST 11, 2022
ACS PHOTONICS
READ

Get More Suggestions >

https://doi.org/10.1021/acsphotonics.2c00774
ACS Photonics 2022, 9, 3366−3373